PAPER • OPEN ACCESS

Scattering of a particle with internal structure from a single slit: exact numerical solutions

New Journal of Physics
The open access journal at the forefront of physics

Deutsche Physikalische Gesellschaft DPG
IOP Institute of Physics

Published in partnership with: Deutsche Physikalische Gesellschaft and the Institute of Physics

OPEN ACCESS

RECEIVED
4 December 2014

ACCEPTED FOR PUBLICATION
13 January 2015

PUBLISHED
13 February 2015

PAPER

Scattering of a particle with internal structure from a single slit: exact numerical solutions

Piroska Dömötör[1,5], Péter Földi[1], Mihály G Benedict[1], Bruce W Shore[2] and Wolfgang P Schleich[3,4]

[1] Department of Theoretical Physics, University of Szeged, H-6720 Szeged, Hungary
[2] 618 Escondido Circle, Livermore, CA 94550, USA
[3] Institut für Quantenphysik and Center for Integrated Quantum Science and Technology (IQST), Universität Ulm, Albert-Einstein-Allee 11, D-89069 Ulm, Germany
[4] Texas A&M University Institute for Advanced Study (TIAS), Institute for Quantum Science and Engineering (IQSE) and Department of Physics and Astronomy, Texas A&M University, College Station, TX 77843-4242, USA
[5] Author to whom any correspondence should be addressed.

E-mail: dpiri@physx.u-szeged.hu, foldi@physx.u-szeged.hu, benedict@physx.u-szeged.hu, bwshore@alum.mit.edu and Wolfgang.Schleich@uni-ulm.de

Keywords: scattering of structured particles, quantum corrections to rotor passage through aperture, Green's function

Abstract

Scattering of a quantum particle with internal structure is fundamentally different from that of a point particle and shows quantum effects such as the modification of transmission due to tunnelling and trapping of the particle. As in a preceding paper (Shore *et al* 2014 *New J. Phys.* **17** 013046) we consider a model of a symmetric, rigid rotor travelling through an aperture in a thin but impenetrable screen which is perpendicular to both the direction of motion and the rotation axis. We determine the quantum mechanical properties of this two-dimensional geometrical model using a quasi one-dimensional scattering problem with unconventional boundaries. Our calculations rely on finding the Green's function, which has a direct connection to the scattering matrix. Evaluated on a discrete lattice the Hamiltonian is 'dressed' by a self-energy correction that takes into account the open boundary conditions in an exact way. We find that the passage through the aperture can be suppressed or enhanced as a result of the rotational motion. These effects manifest themselves through resonances in the transmission probability as a function of incident energy and symmetry of the incident wavefunction. We determine the density-of-states to reveal the mode structure of resonant states and to exhibit the lifetimes of temporary trapping within the aperture.

1. Introduction

In a previous article [1], referred hereafter as article I, we have considered the motion of a structured particle, idealized as a symmetric rigid rotor, passing through an aperture whose size is comparable to the particle. This is an important problem, because there are a number of experimental situations where the internal structure of a quantum mechanical object can play a role: for a list of references see [1]. On the other hand this is an interesting question on its own, as already in the classical picture the relevant coordinates are constrained in a nontrivial way, while in the quantum mechanical treatment this leads to a complicated entanglement of the translational and rotational degrees of freedom. Article I introduced an approximation that decoupled the translational and rotational motions thereby obtaining a set of one-dimensional Schrödinger equations for the hindered translation with effective potentials depending on the rotational mode. The present work removes the simplification made in that work, and provides a method that solves the two-dimensional scattering problem within numerical accuracy.

Our article is organized as follows. In section 2 we summarize the model analyzed in article I. We present the relevant Hamiltonian and the boundary conditions that will determine the wavefunction. Section 3 presents the quantum dynamics as a quasi one-dimensional scattering problem showing analogy to the motion of charge carriers in nanostructures [2]. We use here the technique of the *S* matrix and the Green's function suited to a

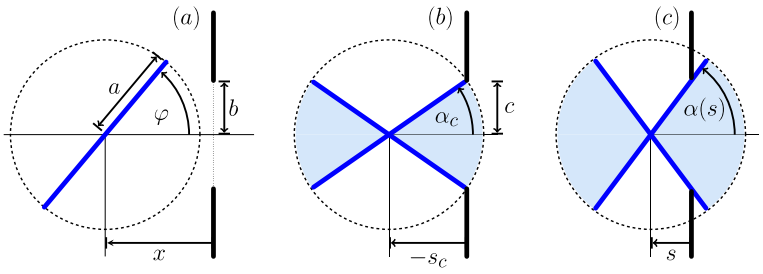

Figure 1. (a) A symmetric rotor of radius a rotating in a plane, approaches an aperture of radius b in a thin screen. The centre-of-mass of the rotor is constrained to move along the symmetry axis of the aperture. This way the centre-of-mass is characterized by a single coordinate x measured along this axis. The other coordinate is the orientation of the rotor, described by the angle φ, with respect to this symmetry axis. The relevant parameter describing the geometrical situation is the aperture-to-length ratio $c \equiv b/a$. The geometrical connection between the centre-of-mass coordinate and allowable rotation angles for a classical rotor passing through the aperture is demonstrated in frames (b) and (c), where we have used the dimensionless coordinate s defined by (4).

numerical solution without the approximations used in article I. We then devote section 4 to the discussion of the results obtained with this technique, paying particular attention to the density-of-states (DOS) and to the transmission probability and its dependence on the classical constraints. Finally section 5 summarizes our results.

In order to keep the article self-contained we place details in appendices. In appendix A we present a derivation of the so-called Fisher–Lee relation that connects elements of the Green's function and the scattering matrix. Appendix B is devoted to the evaluation of the Green's function. Finally, appendix C provides details about the discretization of the scattering problem.

2. The model: a symmetric rigid rotor constrained to a track

In this section we formulate the problem of the quantum mechanical scattering of a rotor from a single slit. Here we are rather brief and refer for a more detailed treatment to article I. As described in article I we consider the passage of a particle with rigid but orientable internal structure, expressible as rotation of a rigid symmetric rod, through a single aperture, in an impenetrable thin screen. The motion takes place in a plane perpendicular to the screen. For further simplification the centre-of-mass motion is constrained to be along the symmetry axis of the aperture. With this assumption we are dealing with a two-dimensional problem characterized by the centre-of-mass coordinate x and angular coordinate φ. (See frame (a) of figure 1 for coordinates and length scales.)

2.1. The two-dimensional Hamiltonian

The classical Hamiltonian for our model problem is the sum of translational and rotational kinetic energies

$$H = \frac{p_x^2}{2M} + \frac{p_\varphi^2}{2\mathcal{M}}, \tag{1}$$

where M is the total mass of the particle and $\mathcal{M}$ is the moment of inertia. We introduce a dimensionless mass-distribution parameter κ to relate M and $\mathcal{M}$

$$\mathcal{M} \equiv M \times (\kappa a)^2, \tag{2}$$

thereby quantifying the distribution of rotor mass. In coordinate representation the quantum-mechanical Hamiltonian obtained from (1) becomes the differential operator

$$H = -\frac{\hbar^2}{2M}\left[\frac{\partial^2}{\partial x^2} + \frac{1}{(\kappa a)^2}\frac{\partial^2}{\partial \varphi^2}\right], \tag{3}$$

and with the dimensionless, scaled parameters of coordinate s and energy ε

$$s \equiv \frac{x}{\kappa a}, \qquad \varepsilon \equiv E\left(\frac{\hbar^2}{2M(\kappa a)^2}\right)^{-1}, \tag{4}$$

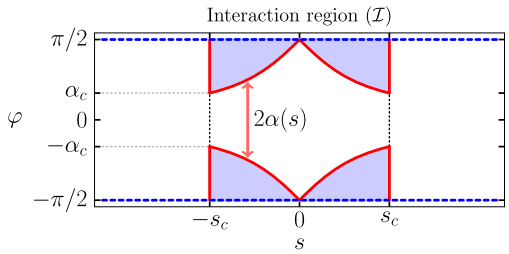

Figure 2. The geometrically allowed (white) and forbidden (shaded) rotation angles φ (vertical axis) as stipulated by (8) in the special case $c \equiv b/a = 0.5$. In the quantum mechanical treatment of section 3 we will prescribe a vanishing wavefunction on the boundary of the classically allowed region (continuous red line), and a π-periodicity in the φ-variable (thick dashed blue line). α_c is defined in (11).

the energy eigenvalue equation is

$$-\left[\frac{\partial^2}{\partial s^2}+\frac{\partial^2}{\partial \varphi^2}\right]\Psi_\varepsilon(s,\varphi)=\varepsilon\,\Psi_\varepsilon(s,\varphi). \tag{5}$$

2.2. Rotational constraints as boundary conditions

The eigenvalue equation (5) is to be completed by boundary conditions. We fix these by adapting the classical geometrical constraints. Classically the effect of the aperture is to hinder rotation as the particle approaches the screen. In frames (b) and (c) of figure 1 we demonstrate the geometrical connection between the centre-of-mass coordinate and the allowable rotation angles.

To characterize the geometry of the rotor relative to the aperture we need, in addition to the parameters κ and ε, the aperture-to-length ratio

$$c \equiv \frac{b}{a}. \tag{6}$$

As seen in figure 1, when the rotor is within the spatial range

$$-s_c \leqslant s \leqslant +s_c, \quad \text{where} \quad s_c \equiv \frac{1}{\kappa}\sqrt{1-c^2}, \tag{7}$$

the rotation angle φ is constrained by the inequalities

$$-\alpha(s) \leqslant \varphi \leqslant \alpha(s), \qquad \text{where} \quad \alpha(s) \equiv \arctan\frac{c}{\kappa|s|}. \tag{8}$$

In the following sections we will refer to this range as the *interaction region* ($\mathcal{I}$).

In figure 2 we show the allowed domains of the angle φ determined by (8). To incorporate the hindered motion and the resulting entanglement of the s and φ variables into the quantum-mechanical description we impose the boundary condition that the wavefunction must vanish at the border of the geometrically allowed angular domain shown as thick red lines in figure 2:

$$\Psi_\varepsilon(s,\varphi=\pm\alpha(s))=0, \qquad \text{for} \quad -s_c \leqslant s \leqslant s_c. \tag{9}$$

In addition the physical configuration of a symmetric rotor, as considered here, is unchanged if it is rotated by π. Due to this symmetry the energy eigenfunctions of the rotor must obey the symmetry relation

$$\Psi_\varepsilon(s,\varphi+\pi)=\pm\Psi_\varepsilon(s,\varphi) \qquad \text{for} \quad -\infty < s < \infty. \tag{10}$$

In figure 2 we denote this π-periodicity by thick dashed blue lines.

2.3. Classical transmission probability

In order to bring out the similarities and differences between classical and quantum mechanical scattering, we consider an ensemble of non-rotating classical particles far away from the aperture, all with fixed initial energy ε and with an orientation angle φ distributed evenly on the interval $-\pi/2 \leqslant \varphi \leqslant \pi/2$.

According to (8) from this stream of classical non-rotating particles only those pass through the aperture whose angle of orientation at $s=-s_c$ satisfies the inequality

$$-\alpha_c \leqslant \varphi \leqslant \alpha_c, \quad \text{where} \quad \alpha_c \equiv \alpha(s_c) \equiv \arctan\frac{c}{\kappa s_c}. \tag{11}$$

For all other angles the classical rotor will be reflected.

We define the geometric transmission probability for the incident rotors as the fraction of the ensemble in which the initial angle φ meets this constraint

$$T^{\mathrm{c}} = \frac{2\alpha_c}{\pi} = \frac{2}{\pi}\arctan\left(\frac{c}{\sqrt{1-c^2}}\right). \tag{12}$$

This *classical* probability depends only on the relative sizes of the rotor and the aperture and is independent of the initial energy ε.

3. The quantum mechanical scattering problem

In this section we briefly review the theoretical background to be used in solving the scattering problem, such as the S matrix, the Green's function, and their connection. For further characterization of the process the concept of the spectral function and the ensuing DOS are also defined.

3.1. Formulation of the scattering problem

We treat the passage of the rotor through the aperture as a *quasi one-dimensional stationary scattering* problem [3], in which an incident wave of fixed energy ε from the left encounters an obstructed passageway shown in figure 2, resulting in transmitted and reflected waves. To ensure this behaviour, we prescribe two additional asymptotic boundary conditions on Ψ_ε.

3.1.1. The free particle

Outside of the interaction region $\mathcal{I}$ the rotor is unaffected by aperture-induced hindrance and the two-dimensional Schrödinger equation (5) is separable into translational and rotational variables

$$\left[\frac{\partial^2}{\partial s^2} + k_m^2\right]\psi_{k_m}^{(\pm)}(s) = 0, \qquad \left[\frac{\partial^2}{\partial \varphi^2} + \varepsilon_m^{(\mathrm{rot})}\right]\phi_m(\varphi) = 0, \tag{13}$$

while the energy eigenvalue ε is the sum of translational and rotational contributions

$$\varepsilon = k_m^2 + \varepsilon_m^{(\mathrm{rot})}. \tag{14}$$

The rotational wavefunctions ϕ_m are either periodic or acquire a '−' sign when the system undergoes a π rotation (10). In this article we restrict our analysis to free particle wavefunctions with π periodic rotational eigenfunctions:

$$\phi_m(\varphi) = \frac{1}{\sqrt{\pi}}\,\mathrm{e}^{\mathrm{i}2m\varphi}, \qquad \varepsilon_m^{(\mathrm{rot})} = 4m^2. \tag{15}$$

Far from the interaction region $\mathcal{I}$ the translational wavefunctions are plane waves

$$\psi_{k_m}^{(\pm)}(s) = \mathrm{e}^{\pm \mathrm{i}k_m s}. \tag{16}$$

For given initial energy ε and rotational state m the wavevector

$$k_m = \sqrt{\varepsilon - 4m^2} \tag{17}$$

is constrained to be a real number. This means that at a fixed total energy ε we have a restricted number of travelling modes given by

$$m_0 \equiv \lfloor \sqrt{\varepsilon}/2 \rfloor, \tag{18}$$

where $\lfloor\ \rfloor$ denotes the integer part.

3.1.2. The asymptotic free domains

The incident wave coming from the left is a two-dimensional partial wave decomposition

$$\Psi_\varepsilon^{\mathrm{in}}(s,\varphi) \equiv \sum_{m=-m_0}^{m_0} c_m\,\mathrm{e}^{\mathrm{i}k_m s}\,\phi_m(\varphi), \tag{19}$$

with complex-valued probability amplitudes c_m, exhibiting the entanglement of the translational and rotational degrees of freedom.

Far away to the left from the interaction region $\mathcal{I}$ the total stationary wavefunction of energy ε is the sum of the incident wave (19) and the resulting reflected wave, with probability amplitudes r_m

$$\Psi_\varepsilon^{\mathrm{L}}(s,\varphi) = \sum_{m=-m_0}^{m_0} \left(c_m \mathrm{e}^{\mathrm{i}k_m s} + r_m \mathrm{e}^{-\mathrm{i}k_m s}\right) \phi_m(\varphi). \tag{20}$$

Far to the right we have a transmitted wave, with transmission coefficients t_m

$$\Psi_\varepsilon^{\mathrm{R}}(s,\varphi) = \sum_{m=-m_0}^{m_0} t_m \, \mathrm{e}^{\mathrm{i}k_m s} \, \phi_m(\varphi). \tag{21}$$

The quantum counterpart of the classical transmission probability T^{c} given by (12) is the transmitted probability current over the incident one

$$T(\varepsilon) = \frac{\sum_{m=-m_0}^{m_0} k_m \, |t_m|^2}{\sum_{m=-m_0}^{m_0} k_m \, |c_m|^2}, \tag{22}$$

which depends on scaled energy ε through the transmission probability amplitudes t_m and the wave vectors k_m.

3.1.3. Connecting the free domains: the S matrix

The linear connection between the incident amplitudes c_m and the outgoing amplitudes r_m and t_m defined by (19)–(21), respectively is most conveniently summarized in the S matrix of the problem. Using labels L and R referring to the far left and right domains outside of $\mathcal{I}$, the elements of the S matrix act as

$$r_m = \sum_n S_{mn}^{\mathrm{LL}} \, c_n, \quad \text{and} \quad t_m = \sum_n S_{mn}^{\mathrm{RL}} \, c_n. \tag{23}$$

Thus to calculate the transmission probability (22) we need to know the S matrices $\mathbf{S}^{\mathrm{LL}}$ and $\mathbf{S}^{\mathrm{RL}}$, respectively[6].

3.2. The Green's function

The most efficient approach to solve the scattering problem involves the Green's function [4], which according to [2] can be physically interpreted as a generalized S matrix describing the response at any point $\mathbf{r}$ due to an excitation at point $\mathbf{r}'$. In coordinate representation the desired Green's function is defined, as a solution of the equation

$$\left[\varepsilon + \mathrm{i}\eta + \frac{\partial^2}{\partial s^2} + \frac{\partial^2}{\partial \varphi^2}\right] G_\varepsilon(s,\varphi;s',\varphi') = \delta(s-s')\delta(\varphi-\varphi'). \tag{24}$$

The positive infinitesimal η with $\eta \longrightarrow 0^+$ ensures that we obtain the *retarded* Green's function, which contains only outgoing waves far to the left and right from $\mathcal{I}$, i.e. that ensures the physically acceptable boundary conditions given by (20) and (21). The Green's function G_ε depends on the scaled energy ε, which we have indicated by a subscript.

In the abstract Hilbert space notation of quantum mechanics the defining equation (24) of the Green's function is an operator equation

$$[(\varepsilon + \mathrm{i}\eta)\mathbf{1} - \mathbf{H}]\,\mathbf{G}(\varepsilon) = \mathbf{1}, \tag{25}$$

where $\mathbf{H}$ is the Hamiltonian of the problem. This form expresses the fact that $\mathbf{G}(\varepsilon)$ is the inverse of the energy minus the Hamiltonian, but this operator inverse should be treated carefully, as $[\varepsilon\mathbf{1} - \mathbf{H}]$ is singular at the eigenvalues of $\mathbf{H}$.

3.3. Partition of the system

The difficulty of the present problem arises from the complicated boundary conditions inside $\mathcal{I}$, as apparent from figure 2 and expressed by (8) and (9). These make the allowed values of the translational coordinate s and the rotation angle φ depend on each other. It is this non-separability that obstructs an exact analytical treatment, although for specific types of low energy incident waves we obtained results in article I by means of analytic approximations.

Rather than introduce analytic simplification, we shall represent the Hamiltonian on a discrete lattice, by using lattice points where the wavefunction is declared to be nonzero. In this discrete representation (25) becomes a system of linear equations for $\mathbf{G}(\varepsilon)$ which can be solved in principle by matrix inversion.

The posed problem is periodic in φ but covers an infinite interval of s so the discrete representation space is still of infinite size. Note that by simply cutting the infinite discrete representation at some point and changing to

[6] Many times in the literature, instead of the S matrix defined in (23), a modified unitary S matrix is used, describing the linear connection between the incoming and outgoing *fluxes*, i.e. probability *current* amplitudes.

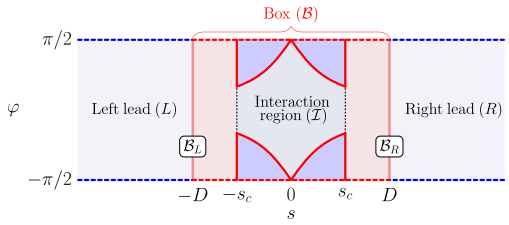

Figure 3. We enclose the interaction region $\mathcal{I}$ in a rectangular box $\mathcal{B}$, outside of which the wavefunction $\Psi_\varepsilon(s,\varphi)$ is expressible as products of unhindered-rotor wave functions $\phi_m(s)$ and companion plane waves $e^{\pm ik_m s}$ given by (20) and (21). Our goal is to obtain numerically exact solutions within the box using a discrete mesh of points.

a finite-size Hamiltonian we would automatically introduce artificial closed boundaries and we would get the Green's function of an *isolated* finite region.

To avoid the isolation, we partition the Hilbert space more carefully into 'left lead + box + right lead' as indicated in figure 3 and incorporate the effect of the leads in the domain of the box in an exact way [2]. We choose the rectangular box $\mathcal{B}$, which encloses the interaction region, in such way that along the left ($\mathcal{B}_\mathrm{L}$) and right ($\mathcal{B}_\mathrm{R}$) boundaries of the box the conditions of (20) and (21) are still valid i.e. we have *open boundary conditions* there.

The idea of dividing the Hilbert space into 'inner' and 'outer' parts and deriving the effect of the 'outer parts' on the 'inner parts' has a long history in many branches of quantum physics [5–8].

3.4. Energy wavefunctions from the Green's function

We next outline how to calculate the wavefunction inside the box (arising from the incident wave) with help of the Green's function, and how to connect the free left and right domains via the S matrix.

3.4.1. Green's function in the box

By projecting equation (25) on the three domains (left lead, box and right lead) and solving for $\mathbf{G}(\varepsilon)$, which when restricted to the box domain will be denoted by $\mathbf{G}^{\mathrm{BB}}(\varepsilon)$, we find according to appendix B the relation

$$\mathbf{G}^{\mathrm{BB}}(\varepsilon) = \left[\varepsilon\mathbf{1} - \mathbf{H}^{\mathrm{BB}} - \mathbf{\Sigma}(\varepsilon)\right]^{-1}. \tag{26}$$

The correction $\mathbf{\Sigma}(\varepsilon)$ to the Hamiltonian $\mathbf{H}^{\mathrm{BB}}$ is known as the *self-energy*. In the work of Feshbach [5, 6] and others this term is a non-Hermitian effective potential. On a discrete lattice this *non-Hermitian* correction can be calculated exactly with the semi-infinite leads on the left and right side (see (C.5)).

3.4.2. The wavefunction in the box

At this point we could proceed to the S matrix without explicit calculation of the wavefunction as is usually done. But for our specific problem the explicit form of the wavefunction inside $\mathcal{B}$ is also interesting. We calculate it from the incident wave (19) and the Green's function inside the Box, using the fact that we have *open boundary conditions* for Ψ_ε at $\mathcal{B}_\mathrm{L}$ and $\mathcal{B}_\mathrm{R}$ which must be inherited by $\mathbf{G}(\varepsilon)$ [9]. For details we refer to appendix A.

With the help of these conditions we evaluate the resulting integral from Green's theorem (A.3), giving the wavefunction inside the box as

$$\Psi^{\mathrm{B}}_\varepsilon(s,\varphi) = \int_{-\pi/2}^{\pi/2} \mathrm{d}\varphi'\; G_\varepsilon(s,\varphi;-D,\varphi')\left[\sum_{m=-m_0}^{m_0} 2ik_m c_m \phi_m(\varphi')\right]. \tag{27}$$

We stress that equation (27) is exact, free of any infinite summation or approximation, and it requires $\mathbf{G}(\varepsilon)$ only in the finite domain $\mathcal{B}$ i.e. $\mathbf{G}^{\mathrm{BB}}(\varepsilon)$. We note that equations of the Lippmann–Schwinger type [10] also express formally Ψ_ε on the full two-dimensional plane [11].

3.4.3. Scattering matrix from the Green's function

Taking only excitations which correspond to incident waves from the left, we relate elements of the S matrix directly to the Green's function evaluated at the left ($\mathcal{B}_\mathrm{L}$) and right ($\mathcal{B}_\mathrm{R}$) boundaries of $\mathcal{B}$. To do so we introduce the notation

$$G^{qp}_\varepsilon\left(\varphi_q;\varphi_p\right) \equiv \left\langle \mathcal{B}_q \right| \mathbf{G}(\varepsilon) \left| \mathcal{B}_p \right\rangle, \tag{28}$$

where the index q and the index p on G can be either L or R. The desired relationship between the blocks of $\mathbf{S}$ and $\mathbf{G}(\varepsilon)$ at the corresponding boundaries takes the form:

$$S_{nm}^{qp} = -\delta_{qp}\delta_{nm} + \mathrm{i}2k_m \int_{-\pi/2}^{\pi/2} \mathrm{d}\varphi_p \int_{-\pi/2}^{\pi/2} \mathrm{d}\varphi_q \, \phi_n^*\left(\varphi_q\right) G_\varepsilon^{qp}\left(\varphi_q;\, \varphi_p\right) \phi_m\left(\varphi_p\right). \tag{29}$$

This relationship is sometimes referred to in the literature as the Fisher–Lee relation [2, 12]. For completeness we outline a simple alternative derivation of equation (29) in appendix A.

3.5. Characterization of the resonances

Due to the presence of the self-energy $\boldsymbol{\Sigma}(\varepsilon)$ the discrete energy spectrum of the isolated box becomes a continuous one, while the eigenstates broaden into resonances [11]. The characteristic features of such an energy spectrum, containing long-living resonant states, are embodied in the spectral function, in the density-of-states (DOS), and in the local density-of-states (LDOS). We now briefly review these concepts.

3.5.1. Lifetimes

To gain more insight into the physics of the Green's function of the box we return for a moment to the energy eigenvalue equation with the effective Hamiltonian (26) . We cannot calculate the solutions of the modified eigenvalue problem

$$\left[\mathbf{H}^{\mathrm{BB}} + \boldsymbol{\Sigma}(\varepsilon)\right] \left|\Psi_\mu^{\mathrm{B}}\right\rangle = \varepsilon_\mu \left|\Psi_\mu^{\mathrm{B}}\right\rangle, \tag{30}$$

as $\boldsymbol{\Sigma}(\varepsilon)$ is itself energy dependent, but we see the double effect of the non-Hermitian correction compared to the eigenvalue equation of the isolated box. The Hermitian part of $\boldsymbol{\Sigma}(\varepsilon)$ simply shifts the eigenenergies $\varepsilon_{\mu,0}$ of the isolated problem, while the anti-Hermitian part brings in an imaginary contribution, resulting in

$$\varepsilon_\mu = \varepsilon_{\mu,0} - \Delta_\mu - \mathrm{i}\left(\gamma_\mu/2\right). \tag{31}$$

The imaginary part leads to an exponential decay of the absolute-value squared wavefunction during time evolution. In this sense $1/\gamma_\mu$ represents the *lifetime* of state $\left|\Psi_\mu^{\mathrm{B}}\right\rangle$.

3.5.2. Spectral function

All the relevant information contained in the solutions of the eigenvalue equation (30) is also contained in the so-called spectral function of the box, defined as [13]

$$\mathbf{A}^{\mathrm{BB}}(\varepsilon) \equiv \mathrm{i}\left[\mathbf{G}^{\mathrm{BB}}(\varepsilon) - \left(\mathbf{G}^{\mathrm{BB}}(\varepsilon)\right)^\dagger\right] = -2\,\mathrm{Im}\left[\mathbf{G}^{\mathrm{BB}}(\varepsilon)\right]. \tag{32}$$

Using the formal eigenfunction expansion

$$\mathbf{G}^{\mathrm{BB}}(\varepsilon) = \sum_\mu \frac{1}{\varepsilon - \varepsilon_\mu} \left|\Psi_\mu^{\mathrm{B}}\right\rangle \left\langle\Psi_\mu^{\mathrm{B}}\right| \tag{33}$$

arising from (30) with the energies given by (31), from (32) we obtain in the abstract Hilbert space notation the relation [2]

$$\mathbf{A}^{\mathrm{BB}}(\varepsilon) = \sum_\mu \left|\Psi_\mu^{\mathrm{B}}\right\rangle \left\langle\Psi_\mu^{\mathrm{B}}\right| \frac{\gamma_\mu}{\left(\varepsilon - \varepsilon_{\mu,0} + \Delta_\mu\right)^2 + \left(\gamma_\mu/2\right)^2}. \tag{34}$$

3.5.3. Density-of-states (DOS)

The energy spectrum of the system is characterized by the DOS $\mathcal{N}(\varepsilon)$, defined as the trace of the spectral function $\mathbf{A}^{\mathrm{BB}}(\varepsilon)$

$$\mathcal{N}(\varepsilon) \equiv \frac{1}{2\pi}\,\mathrm{Tr}\left[\mathbf{A}^{\mathrm{BB}}(\varepsilon)\right] = \frac{1}{2\pi}\int_{\mathcal{B}} \mathrm{d}\mathbf{r}\, \langle \mathbf{r} \mid \mathbf{A}^{\mathrm{BB}}(\varepsilon) \mid \mathbf{r}\rangle. \tag{35}$$

With help of (34) we can understand the definition in (35) as [2]

$$\mathcal{N}(\varepsilon) = \frac{1}{\pi}\sum_\mu \frac{\gamma_\mu/2}{\left(\varepsilon - \varepsilon_{\mu,0} + \Delta_\mu\right)^2 + \left(\gamma_\mu/2\right)^2}. \tag{36}$$

This function exhibits a succession of peaks as a function of the scaled energy ε, corresponding to small values of γ_μ, i.e. to long lifetime states $\left|\Psi_\mu^{\mathrm{B}}\right\rangle$. The locations of these peaks, apparent from the Lorentzian in (36), are the energies where we expect to see resonances in the transmission. In the limit of infinitely long lifetimes the DOS

approaches a succession of Dirac delta functions

$$\lim_{\gamma_\mu \to 0} \mathcal{N}(\varepsilon) = \sum_\mu \delta\left(\varepsilon - \varepsilon_{\mu,0} + \Delta_\mu\right). \tag{37}$$

3.5.4. Local density-of-states (LDOS)

The LDOS gives us more insight into the nature of the peaks in $\mathcal{N}(\varepsilon)$. This state-dependent function is defined as the spectral function (32) evaluated in coordinate representation for diagonal elements $\mathbf{r}$ in $\mathcal{B}$

$$\rho_\varepsilon(\mathbf{r}) \equiv \frac{1}{2\pi}\langle \mathbf{r} \mid \mathbf{A}^{\mathrm{BB}}(\varepsilon) \mid \mathbf{r}\rangle = \frac{1}{2\pi}\sum_\mu \left|\Psi_\mu^{\mathrm{B}}(\mathbf{r})\right|^2 \frac{\gamma_\mu}{\left(\varepsilon - \varepsilon_{\mu,0} + \Delta_\mu\right)^2 + \left(\gamma_\mu/2\right)^2}. \tag{38}$$

For infinite lifetimes this expression tends to

$$\lim_{\gamma_\mu \to 0} \rho_\varepsilon(\mathbf{r}) = \sum_\mu \left|\Psi_\mu^{\mathrm{B}}(\mathbf{r})\right|^2 \delta\left(\varepsilon - \varepsilon_{\mu,0} + \Delta_\mu\right). \tag{39}$$

In this limit the LDOS $\rho_\varepsilon(\mathbf{r})$ provides the spatial distribution of the probability density of the resonant states.

4. Numerical results

In this section we present numerical solutions of the scattering problem posed in section 3 for several values of the aperture-to-length ratio and for different incident wave symmetries. Notable is the presence of scattering resonances, in which the rotor undergoes temporary trapping within the interaction region $\mathcal{I}$. Besides the calculation of the transmission probability (22) we also analyze this phenomenon with the aid of the concepts introduced in subsection 3.5.

We have carried out the calculation on a discrete lattice with 49×49 lattice points corresponding to a box $\mathcal{B}$ of size $[-\pi/2,\ \pi/2] \times [-\pi/2,\ \pi/2]$ in the dimensionless coordinates s and φ. We chose this interval by refining the grid until we saw convergence in the results. The energy range investigated runs between 0 and $50E_0$, where $E_0 \equiv \hbar^2/2M(\kappa a)^2$ is the elementary unit of rotational excitation for our rotor. This range corresponds to 'cold' molecules, where we expect specific quantum effects.

4.1. Identification of the true resonances

According to (36) a plot of $\mathcal{N}(\varepsilon)$ will reveal peaks corresponding to energies where long-living resonant states occur. For some of these peaks there is a concentration of probability (quasi-bound resonant states) within the region $\mathcal{I}$. Other peaks occur as a consequence of the dimensions of the box $\mathcal{B}$. We identify the latter by shifting the box $\mathcal{B}$ with respect to $\mathcal{I}$ along the *s*-axis. Such a shift will have little effect on the peaks corresponding to $\mathcal{I}$, while peaks due to the surrounding box will noticeably change.

Frame (*a*) of figure 4 shows an example of the energy variation of the DOS $\mathcal{N}(\varepsilon)$. The plot reveals a series of peaks—resonances—as well as lesser variations. To clarify the nature of the resonances we have shifted the bounding box $\mathcal{B}$ along the *s*-axis to cover the interval $[-\pi/2,\ \pi/2] + n \cdot [\Delta s,\ \Delta s]$ with $n = 0,\ 1,\ \cdots,\ 6$. Frame (*b*) shows the resulting DOS variation. In this process out of the several peaks only the resonances denoted with solid lines did not change their position and height.

From this procedure we learn that out of the eight peaks shown in frame (*a*) only six are characteristic of $\mathcal{I}$. We denote them as ε_i, with or without a tilde. The energies ε_i ($\tilde{\varepsilon}_i$) will turn out to correspond to even (odd) angular symmetry of the incident wavefunction, respectively. This question of symmetry is discussed in section 4.3.

We emphasize that the size and position of the box $\mathcal{B}$ along the *s* axis does not change the transmission properties of the system because the *S* matrix is invariant under the 'box-shifting' transformation. This gives an additional possibility to verify the precision and validity of the numerical procedure.

4.2. DOS and LDOS

Information about the wavefunctions corresponding to resonant energies comes from the LDOS $\rho_\varepsilon(\mathbf{r})$. Formulae (38) and (39) show that a long-living resonance has a LDOS proportional to the square of the probability distribution of that state, $|\Psi_\mu^{\mathrm{B}}(\mathbf{r})|^2$. We expect that long-living states whose properties are insensitive to the size and location of the box $\mathcal{B}$ will be localized within the interaction region $\mathcal{I}$. Figure 5 verifies this expectation, indeed the first two peaks of $\mathcal{N}(\varepsilon)$ are associated with dominant concentration of probability within $\mathcal{I}$. In contrast, panels corresponding to dotted energy values belong to probability concentration outside of $\mathcal{I}$ but within $\mathcal{B}$. This feature confirms that these energies are not characteristic of $\mathcal{I}$.

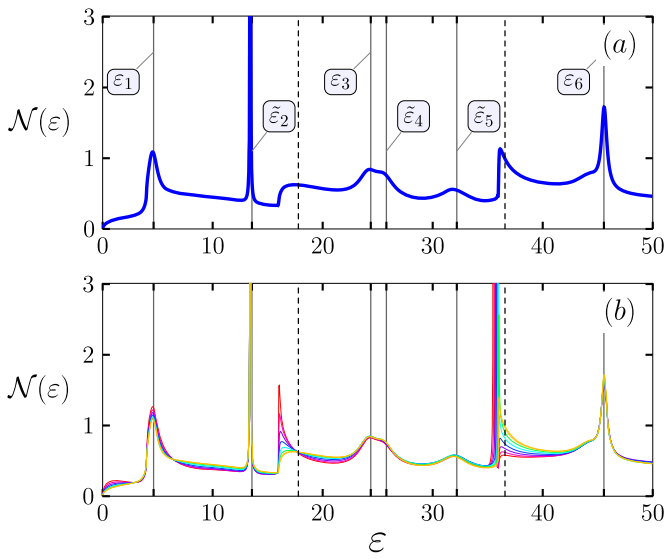

Figure 4. Identification of the true resonances. (*a*) Density-of-states $\mathcal{N}(\varepsilon)$ as a function of scaled energy ε for aperture-to-length ratio $c = 0.5$ and mass-distribution parameter $\kappa = 1$. Peaks correspond to resonant states with longer lifetimes. (*b*) $\mathcal{N}(\varepsilon)$ for shifts of box $\mathcal{B}$ along the s-axis to the range $[-\pi/2, \pi/2] + n \cdot [\Delta s, \Delta s]$ with $n = 0, 1, \cdots, 6$. Dotted vertical lines mark peak positions that changed substantially, in contrast to the true resonances, which do not change much. Out of the eight peaks shown in frame (*a*) only six are characteristic of $\mathcal{I}$. We denote them by ε_i and $\tilde{\varepsilon}_i$. At the resonances ε_i the spatial symmetry of the wavefunction is even while at $\tilde{\varepsilon}_i$ it is odd. The second peak from the left, labelled $\tilde{\varepsilon}_2$, is associated with a long-living resonant state of the system, as follows from its narrow width. From the height of the peak we deduce that the state has a lifetime more than ten times longer than the lifetime of any other state.

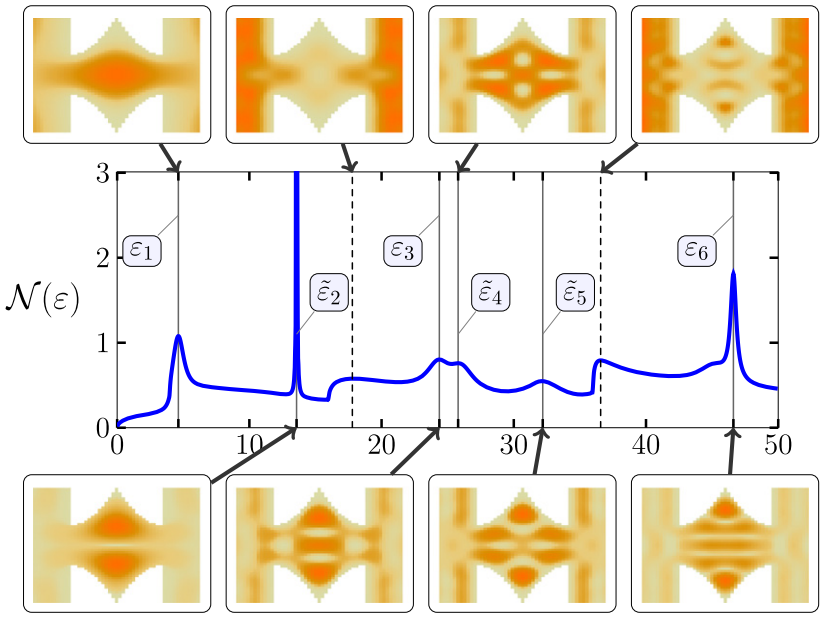

Figure 5. Density-of-states $\mathcal{N}(\varepsilon)$ as a function of scaled energy ε for aperture-to-length ratio $c = 0.5$ and mass-distribution parameter $\kappa = 1$. Above and below we show the density plots of the local density-of-states $\rho_\varepsilon(\mathbf{r})$ for eight selected energies. For narrow resonances $\rho_\varepsilon(\mathbf{r})$ is the probability density. The first two plots belonging to ε_1 and ε_2 display strong concentration within $\mathcal{I}$. The second peak is much sharper than all the other ones and its wavefunction exhibits a single horizontal node. The second and fourth upper panel, that correspond to energy values marked by dotted lines, exhibit concentration within $\mathcal{B}$ but outside of $\mathcal{I}$. This feature identifies these peaks as artefacts of the box $\mathcal{B}$. The other peaks show additional nodal structures in both s and φ, becoming more complicated with increasing energy.

In order to exhibit energies at which long-living states appear, we present in figure 6 the DOS $\mathcal{N}(\varepsilon)$ by a contour plot as a function both of scaled energy ε and of aperture-to-length parameter c. This picture extends the results shown in frame (*a*) of figure 4 for a single value of $c = 0.5$ to a wide range of aperture-to-length parameter values. The white domains for lower c values (lower right part of the contour plot) indicate that for higher energies new long-living resonant states may appear.

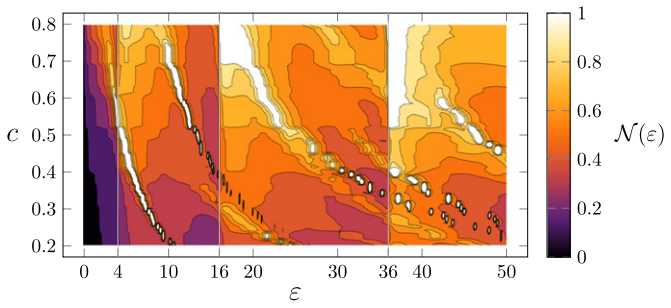

Figure 6. Contour plot of the density-of-states $\mathcal{N}(\varepsilon)$ as a function of scaled energy ε and aperture-to-length parameter c for mass-distribution parameter $\kappa = 1$. Lighter colours denote longer lifetimes. The vertical white lines show energies where the number of travelling modes i.e. $2m_0 + 1$, restricted by condition (18), increases. We can follow how the first two peaks, denoted with ε_1 and $\tilde{\varepsilon}_2$ for $c = 0.5$ in figures 4 and 5, increase and sharpen with decreasing c. In addition, below $c = 0.4$ two new long-living states appear for higher energies.

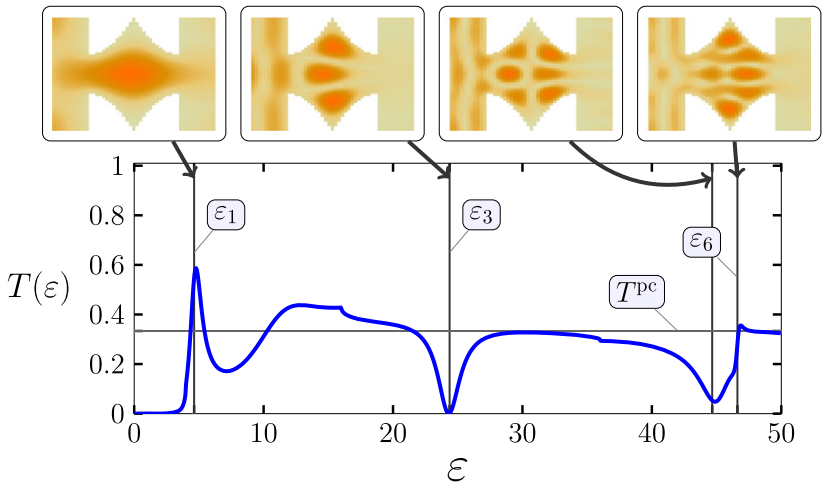

Figure 7. Transmission probability $T(\varepsilon)$ as a function of scaled energy ε for the 'non-rotating' incident state (41). Vertical lines indicate the energies where resonance effects are expected from the density-of-states $\mathcal{N}(\varepsilon)$ shown in figure 5. The horizontal line shows the pseudo-classical transmission probability (40) and $T(\varepsilon)$ varies around this line. The four contour plots correspond to the resonant energies and show the probability-densities $\left|\Psi^{\mathrm{B}}\right|^2$ calculated from (27). Parameters are $c = 0.5, \kappa = 1$.

4.3. Transmission for different rotational modes

In this section we examine how the transmission probability (22) depends on the choice of the incident wavefunction (19). In section 4.1 we used the DOS to identify the energies where resonances appear. Depending on the rotational symmetry of the incoming mode we can identify two essentially different types of transmission behaviour. Incident wavefunctions with *odd* or *even symmetry* in the φ variable will excite different resonance energies.

In order to reveal the genuine quantum effects in the scattering process, we introduce a slight generalization of the classical transmission probability T^{c} defined by (12). We regard the absolute-value square of the φ-dependent part of the incident wavefunction (19) as a distribution of incoming angles for an ensemble of rotors. Accordingly we define the *pseudo-classical transmission probability* by the overlap between the incident distribution and the opening of the interaction region, as given by the integral

$$T^{\mathrm{pc}} \equiv \int_{-\alpha_c}^{\alpha_c} \mathrm{d}\varphi \left| \sum_{m=-m_0}^{m_0} c_m \, \phi_m(\varphi) \right|^2 . \tag{40}$$

In figures 7 and 9 a horizontal line marks this pseudo-classical transmission probability. One expects that for higher energies the quantum mechanical transmission probability (22) should saturate to this value.

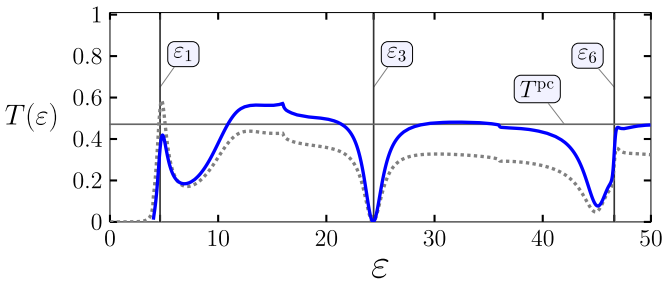

Figure 8. Transmission probability $T(\varepsilon)$ as a function of scaled energy ε for the even example of (42). For comparison the result for the non-rotating incident-wave is also shown (dashed grey line). The two curves show the same overall characteristics. Parameters are $c = 0.5, \kappa = 1$.

4.3.1. Even incident waves

In the present subsection we consider incident waves which are *even* in the φ variable, giving rise to the symmetry relation $c_m = c_{-m}$ in (19). The most elementary examples in the low energy range are

$$\Psi_0^{\rm even}(s, \varphi) = {\rm e}^{{\rm i}k_0 s}\phi_0(\varphi) = {\rm e}^{{\rm i}k_0 s}\frac{1}{\sqrt{\pi}}, \tag{41}$$

$$\Psi_1^{\rm even}(s, \varphi) = {\rm e}^{{\rm i}k_1 s}\frac{1}{\sqrt{2}}\Big[\phi_1(\varphi) + \phi_{-1}(\varphi)\Big] = {\rm e}^{{\rm i}k_1 s}\sqrt{\frac{2}{\pi}}\cos(2\varphi). \tag{42}$$

The example of (41), taking only the $m = 0$ term, corresponds to a non-rotating molecule, which was the main subject of article I. We note that in this special case the pseudo-classical transmission probability (40) is equal to the classical one (12). We present numerical results of the non-rotating case in figure 7. These justify the conclusions of article I and show the validity regime of the approximations used there.

Exactly at the first resonant energy ε_1 identified from the DOS we see a peak in the transmission, as well. The position and character of this peak is well described by the analytic calculations in article I.

An other interesting effect is the transmission minimum, implying total reflection, at the third resonance energy ε_3. Such minima are not predicted by the approximation of mode decoupling used in article I and that approximation must be abandoned as the energy increases. The second upper panel of figure 7 corresponding to ε_3, gives a hint for the reason of no transmission. When coupled to the incident wave, the symmetry with respect to the s-axis gets deformed, the wavefunction vanishes at $\mathcal{B}_{\rm R}$ and nothing can get through to the right side.

Figure 8 shows the comparison of the transmissions for incident waves (41) and (42), which exhibit the same overall characteristics. This statement also holds for other possible incident waves with even symmetry in φ, which suggests that the positions and the shapes of the peaks and dips in the transmission are characteristic of the incident wave symmetry with respect to φ.

4.3.2. Odd incident wave

Next we consider incident waves which are *odd* in the φ variable, which corresponds to the symmetry relation $c_m = -c_{-m}$ in equation (19). The most elementary example in the energy regime $\varepsilon < 50$ reads

$$\Psi_1^{\rm odd}(s, \varphi) = {\rm e}^{{\rm i}k_1 s}\frac{1}{\sqrt{2}}\Big[\phi_1(\varphi) - \phi_{-1}(\varphi)\Big] = {\rm i}{\rm e}^{{\rm i}k_1 s}\sqrt{\frac{2}{\pi}}\sin(2\varphi). \tag{43}$$

Note that this incident wave is only possible for energies $\varepsilon > 4$, and this is the only possibility to create an odd incident-wave in the energy regime $4 < \varepsilon \leqslant 16$.

Looking at the lower left panel in figure 5 we see that the long-living resonant state at energy $\tilde{\varepsilon}_2$ has just this odd symmetry. The effect of this resonant state appears in the transmission plot of figure 9 as a very narrow and high peak exactly at $\tilde{\varepsilon}_2$. Otherwise there is almost no transmission for the odd incident wave (43) in the $4 < \varepsilon < 20$ energy range. From the probability-densities $\left|\Psi^{\rm B}\right|^2$ at $\tilde{\varepsilon}_2$, shown in the first upper panel of figure 9, we recognize that with this odd superposition of incident modes it is possible to excite the long-living resonant state at $\tilde{\varepsilon}_2$ whose existence appeared in the DOS in figure 4. It is also possible to excite this state with one of the two rotating mode functions $\phi_{-1}(\varphi)$ or $\phi_1(\varphi)$. However, the odd superposition given by (43) results in a significantly reduced overall transmission except for the resonance at $\tilde{\varepsilon}_2$, which shows up therefore more sharply.

Enhancement of transmission appears also at $\tilde{\varepsilon}_4$ and $\tilde{\varepsilon}_5$, the wavefunction for these energies are also shown in figure 9.

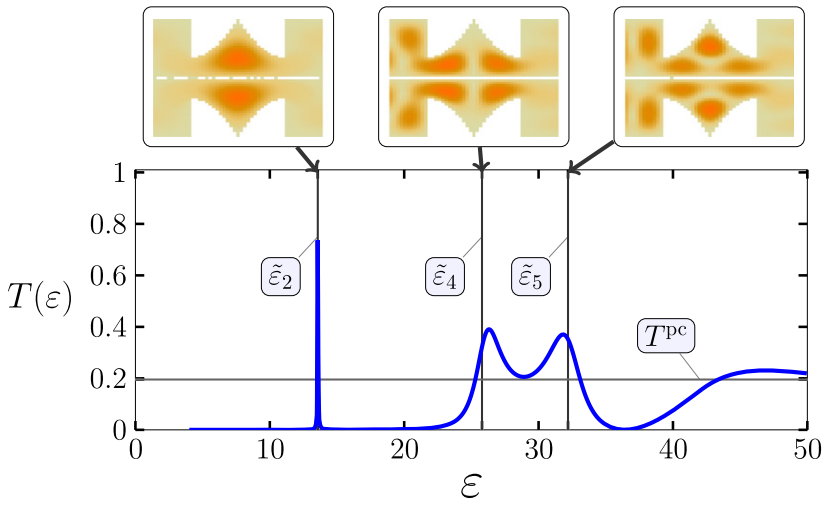

Figure 9. Transmission probability $T(\varepsilon)$ as a function of scaled energy ε for the odd incident wave (43). Vertical lines indicate energies where resonance effects are expected. The horizontal line shows the pseudo-classical transmission probability (40) and $T(\varepsilon)$ for higher energies varies around this line. Above are the three contour plots of wavefunction probability-densities $\left|\Psi^{\mathrm{B}}\right|^2$ corresponding to the resonant energies. Parameters are $c = 0.5, \kappa = 1$.

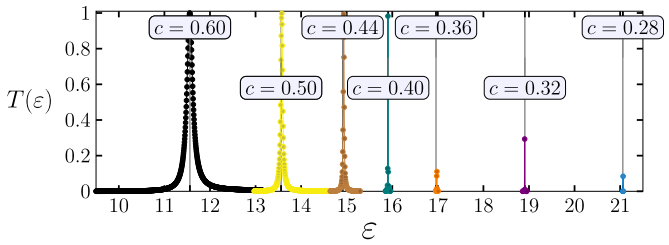

Figure 10. The position of the first transmission peak of the odd incident-wave (43) for seven values of the aperture-to-length parameter c. Vertical lines show the resonant energies deduced from the corresponding maxima in the DOS. As we see, these energies coincide perfectly with the peak maxima of *transmission*.

4.4. A true bound state of the system

In this section we examine the long-living resonance we have found for $c = 0.5$ at $\tilde{\varepsilon}_2 = 13.57$ in the DOS (figure 5). In section 4.3.2 we demonstrated that this state causes a sharp peak in the transmission plot for incident waves with odd symmetry (figure 9). We shall now consider how the transmission peak varies with the aperture-to-length ratio c.

Indeed, the position of this resonance should depend on the value of the parameter c as apparent in figure 6. In figure 10 we show that the transmission maxima coincide perfectly the resonant energies deduced from the DOS. We also see that as the size of the opening gets smaller i.e. as c decreases the transmission is diminishing and finally below $c = 0.27$ no transmission is possible.

No transmission, however, does not mean that the corresponding resonant state can not be excited through the small opening by the incident wave. In figure 11 we show the absolute value square of the wavefunction inside $\mathcal{B}$ in case of the odd incident wave for $c = 0.27$. We see that the long-living state builds up exactly at the resonant-energy, although—as we said before—its existence is not visible in the transmission i.e. it does not couple to the right lead.

Figure 12 shows the approximate lifetimes of this specific resonance as a function of c. We saw already in figure 4 for $c = 0.5$ that this state has a much longer lifetime than any other possible state.

The very narrow and finally disappearing transmission peaks and extremely long lifetimes suggest that around the parameter value $c = 0.3$ the corresponding state is a true bound state of the interaction region ($\mathcal{I}$).

5. Conclusions

In the present article we have investigated a model describing the stationary scattering problem of a rotating cold diatomic molecule passing through an aperture in a restricted two-dimensional geometry. We have calculated

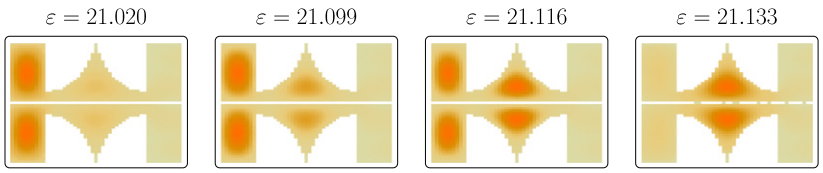

Figure 11. Build-up of the long-living resonant state inside region $\mathcal{I}$ for the odd incident-wave of (43) for the aperture-to-length parameter value $c = 0.27$. At the resonant energy $\varepsilon = 21.133$ the corresponding wavefunction is located almost completely inside $\mathcal{I}$ and supports zero transmission probability.

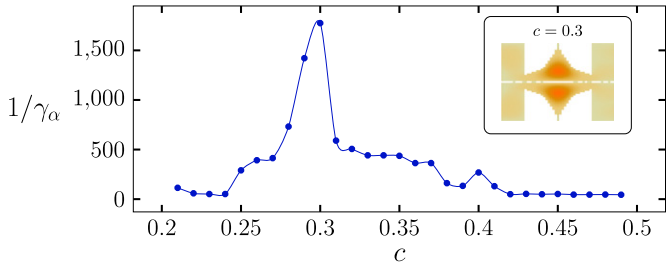

Figure 12. Lifetimes of the long-living resonant state as the c parameter changes. The values of the corresponding maxima shown in the density-of-states plot of figure 6 (denoted with $\tilde{\varepsilon}_2$ for $c = 0.5$), determine the approximate lifetime for the resonant state (36). Time is measured in units of $\frac{2Ma^2}{\hbar}$ (4).

the transmission and the reflection coefficients as functions of the energy for different rotating modes of the incoming molecule. The calculations were carried out by a numerical method based on the Green's function of the problem in a discrete lattice representation. The complicated boundary conditions were taken into account by modifying the Hamiltonian with appropriate self-energy corrections.

We have found resonances in the DOS which could be classified according to the rotational symmetry of the incident wavefunction. Very sharp resonances, corresponding to long-living quasi-bound resonant states, appear. The energies and lifetimes of these resonant states depend on the aperture-to-length ratio c and the rotational symmetry properties of the incident wave.

As the aperture gets smaller than the size of the rotating molecule, the resonance peaks in the transmission get narrower and finally disappear while the lifetime of the corresponding excited state increases indefinitely, suggesting that we have found a true bound state of the system.

Acknowledgments

We thank B Dietz, I Gyémánt, Gy Papp, E Sadurní and G Süssmann for many stimulating discussions. We gratefully acknowledge funding from the Baden-Württemberg Stiftung through the Atomics Program, from the SFB/TR21 'Control of quantum correlations in tailored matter: common perspectives of mesoscopic systems and quantum gases' and from the EU through the research and training network EMALI (MRTN-CT-2006-035369).

The work of PD, PF and MGB was supported by the Hungarian Scientific Research Fund (OTKA) under Contract No. T81364, and by the European Union and the European Social Fund through projects TAMOP-4.2.2.C-11/1/KONV-2012-0010 and TAMOP-4.2.2.A-11/1/KONV-2012-0060.

WPS thanks the Alexander von Humboldt Stiftung and the Max Planck-Gesellschaft for receiving the Max Planck-Forschungspreis. Moreover, he is grateful to Texas A&M University for a Texas A&M University Institute for Advanced Study (TIAS) Faculty Fellowship.

Appendix A. Fisher–Lee relation

Fisher and Lee [12], who deal with charge carriers in nano structures, derive a relationship between the elements of the S matrix and the Green's function of the scattering problem. We present here an alternative derivation, based on Green's theorem, yielding also the wavefunction within the box.

A.1. Wavefunction inside the box $\mathcal{B}$

We denote by $\mathbf{r}$ a point inside the volume bounded by the closed $(s,\ \varphi)$ surface $\mathcal{S}$, and within that domain we choose $G(\mathbf{r},\ \mathbf{r}')$ so that $\Psi(\mathbf{r})$ obeys physically acceptable boundary conditions, i.e. an incident wave from the left is scattered by the structure inside $\mathcal{B}$. We start with Green's second identity [14, 15] applied to the wavefunction and the corresponding Green's function for the domain $\mathcal{B}$. From

$$\left(\Delta_{\mathbf{r}} + \varepsilon\right)\Psi_\varepsilon(\mathbf{r}) = 0, \quad \text{and} \quad \left(\Delta_{\mathbf{r}} + \varepsilon\right)G_\varepsilon\left(\mathbf{r},\ \mathbf{r}'\right) = \delta\left(\mathbf{r} - \mathbf{r}'\right), \tag{A.1}$$

where $\Delta_{\mathbf{r}}$ is the Laplacian, we have

$$\Psi_\varepsilon(\mathbf{r}) = \oint_{\mathcal{S}} \mathrm{d}\mathbf{r}'\left[\Psi_\varepsilon\left(\mathbf{r}'\right)\frac{\partial G_\varepsilon(\mathbf{r},\ \mathbf{r}')}{\partial \mathbf{n}'} - G_\varepsilon\left(\mathbf{r},\ \mathbf{r}'\right)\frac{\partial \Psi_\varepsilon\left(\mathbf{r}'\right)}{\partial \mathbf{n}'}\right]. \tag{A.2}$$

For the evaluation of (A.2) we use the fact that we have periodic boundary conditions at $\varphi = \pm\pi/2$, and so we get a formula containing an integration only over the angular variable:

$$\Psi_\varepsilon(s,\ \varphi) = \int_{-\pi/2}^{\pi/2}\mathrm{d}\varphi'\left[\Psi_\varepsilon(s',\ \varphi')\frac{\partial G_\varepsilon(s,\ \varphi;\ s',\ \varphi')}{\partial s'} - G_\varepsilon(s,\ \varphi;\ s',\ \varphi')\frac{\partial \Psi_\varepsilon(s',\ \varphi')}{\partial s'}\right]\Bigg|_{-D}^{D}. \tag{A.3}$$

With the help of the boundary conditions at the left and right edges we eliminate $\Psi_\varepsilon(s',\ \varphi')$ from the right-hand side of (A.3) and express the wavefunction inside the box solely by the Green's function. Using the complete orthonormal set of the $\phi_m(\varphi)$ mode functions we expand $\Psi_\varepsilon(s,\ \varphi)$ as

$$\Psi_\varepsilon(s,\ \varphi) = \sum_{m=-\infty}^{\infty}\psi_m(s)\,\phi_m(\varphi) \quad \text{with} \quad \psi_m(s) \equiv \int_{-\pi/2}^{\pi/2}\mathrm{d}\varphi\ \phi_m^\star(\varphi)\ \Psi_\varepsilon(s,\ \varphi). \tag{A.4}$$

In other words we do a change of representation, from the $|s,\ \varphi\rangle$ basis to the $\left|s,\ \phi_m\right\rangle$ one, so that we can then exploit the boundary conditions for each mode function separately. We take (19) as the incident wave on the left and readily verify that the $\psi_m(s)$ of the incident wave, with $m = -m_0,\ \cdots,\ m_0$, obey the following inhomogeneous boundary conditions:

$$\frac{\partial\psi_m(s)}{\partial s}\bigg|_{-D} + \mathrm{i}k_m\psi_m(-D) = 2\mathrm{i}k_m c_m, \qquad \frac{\partial\psi_m(s)}{\partial s}\bigg|_{D} - \mathrm{i}k_m\psi_m(D) = 0. \tag{A.5}$$

We denote the Green's function in this representation as $G_{nm}(s;\ s')$ defined by

$$G_{nm}(s;\ s') \equiv \int_{-\pi/2}^{\pi/2}\mathrm{d}\varphi\int_{-\pi/2}^{\pi/2}\mathrm{d}\varphi'\ \phi_n^\star(\varphi)\ G_\varepsilon(s,\ \varphi;\ s',\ \varphi')\ \phi_m(\varphi'). \tag{A.6}$$

As explained in [9] the Green's function inherits the homogeneous version of the boundary conditions for the wavefunction (A.5):

$$\frac{\partial G_{nm}(s;\ s')}{\partial s'}\bigg|_{-D} + \mathrm{i}k_m G_{nm}(s;\ -D) = 0, \qquad \frac{\partial G_{nm}(s;\ s')}{\partial s'}\bigg|_{D} - \mathrm{i}k_m G_{nm}(s;\ D) = 0. \tag{A.7}$$

We expand $\Psi_\varepsilon(s',\ \varphi')$ as (A.4) on the right-hand side of (A.3). Note that we must have a finite sum by continuity, as $\Psi_\varepsilon(s',\ \varphi')$ is evaluated on the left and right boundary where (20) and (21) are also valid. Then multiplying both sides of the expression resulting from (A.3) with $\phi_n(\varphi)$ and integrating over the φ variable we obtain:

$$\psi_n(s) = \sum_{m=-m_0}^{m_0}\left[\psi_m(s')\frac{\partial G_{nm}(s;\ s')}{\partial s'} - G_{nm}(s;\ s')\frac{\partial\psi_m(s')}{\partial s'}\right]\Bigg|_{-D}^{D}. \tag{A.8}$$

Then using the boundary conditions (A.5) and (A.7) we evaluate the necessary partial derivatives at $s' = -D$ and D on the right-hand side of (A.8) cancelling almost everything and leaving us with:

$$\psi_n(s) = \sum_{m=-m_0}^{m_0} G_{nm}(s;\ -D)\ 2\mathrm{i}k_m c_m. \tag{A.9}$$

Now using again the expansion (A.4) and the definition (A.6) of $G_{nm}(s;\ -D)$ plus completeness of the $\phi_n(\varphi)$ mode functions we get a formula for the wavefunction inside $\mathcal{B}$. It is determined by the retarded Green's function of the problem evaluated in $\mathcal{B}$

$$\Psi_{\varepsilon}^{\mathrm{B}}(s,\varphi) = \int_{-\pi/2}^{\pi/2} \mathrm{d}\varphi'\; G_{\varepsilon}(s,\varphi;-D,\varphi') \left[\sum_{m=-m_0}^{m_0} 2\mathrm{i}k_m c_m \phi_m(\varphi') \right]. \tag{A.10}$$

A.2. *S* matrix elements

Using the expansion introduced in (A.4) the wavefunction on the left side of $\mathcal{B}$ (20) has translational part:

$$\psi_n^{\mathrm{L}}(s) = c_n\; \mathrm{e}^{\mathrm{i}k_n(s+D)} + r_n\; \mathrm{e}^{-\mathrm{i}k_n(s+D)}, \qquad (s \leqslant -D), \tag{A.11}$$

while the wavefunction on the right side of $\mathcal{B}$ (21) is represented as

$$\psi_n^{\mathrm{R}}(s) = t_n\; \mathrm{e}^{\mathrm{i}k_n(s-D)}, \qquad (s \geqslant D). \tag{A.12}$$

Note that for both regions we have introduced overall phase factors $\mathrm{e}^{\pm \mathrm{i}k_n D}$, which is equivalent to using different coordinate systems for the left and right leads having their origins at the respective ends of the leads. This change has no effect on the transmission and reflection coefficients containing only the absolute values of the r_n and t_n amplitudes.

According to the definition of the *S* matrix elements (23) the right-hand side of equations (A.11) and (A.12) are:

$$\psi_n^{\mathrm{L}}(s) = \sum_{m=-m_0}^{m_0} \left[\mathrm{e}^{\mathrm{i}k_n(s+D)}\; \delta_{nm} + \mathrm{e}^{-\mathrm{i}k_n(s+D)}\; S_{nm}^{\mathrm{LL}} \right] c_m, \tag{A.13}$$

$$\psi_n^{\mathrm{R}}(s) = \sum_{m=-m_0}^{m_0} \mathrm{e}^{\mathrm{i}k_n(s-D)}\; S_{nm}^{\mathrm{RL}}\; c_m. \tag{A.14}$$

Comparing these equations with (A.9) and demanding continuity at $s = -D$ and D we have the required connection between the elements of the scattering matrix $\mathbf{S}$ and the Green's function of the problem

$$S_{nm}^{\mathrm{LL}} = -\delta_{nm} + 2\mathrm{i}k_m\; G_{nm}(-D,-D), \tag{A.15}$$

$$S_{nm}^{\mathrm{RL}} = 2\mathrm{i}k_m\; G_{nm}(D,-D). \tag{A.16}$$

We evaluate G_{nm} according to (A.6) and see that this is the Fisher–Lee formula (29).

Appendix B. Green's function of the finite region; the self-energy correction

Formally we express the partition introduced in section 3.3 through the projector decomposition of identity

$$\mathbf{1} = |\mathrm{L}\rangle\langle\mathrm{L}| + |\mathrm{B}\rangle\langle\mathrm{B}| + |\mathrm{R}\rangle\langle\mathrm{R}|, \tag{B.1}$$

where $|\mathrm{L}\rangle\langle\mathrm{L}|$, $|\mathrm{B}\rangle\langle\mathrm{B}|$ and $|\mathrm{R}\rangle\langle\mathrm{R}|$ project on subspaces of functions with support in the domains of left lead, box, and right lead, respectively.

Inserting (B.1) in (25) and multiply from the right with $|\mathrm{B}\rangle$ we obtain

$$[(\varepsilon + \mathrm{i}\eta)\mathbf{1} - \mathbf{H}]\{|\mathrm{L}\rangle\langle\mathrm{L}| + |\mathrm{B}\rangle\langle\mathrm{B}| + |\mathrm{R}\rangle\langle\mathrm{R}|\}\mathbf{G}(\varepsilon)\;|\mathrm{B}\rangle = \mathbf{1}\;|\mathrm{B}\rangle. \tag{B.2}$$

Then we calculate projections of this operator equation on the three domains giving

$$\left[(\varepsilon + \mathrm{i}\eta)\mathbf{1} - \mathbf{H}^{\mathrm{LL}}\right]\mathbf{G}^{\mathrm{LB}} + \left(\boldsymbol{\tau}^{\mathrm{L}}\right)^{\dagger}\mathbf{G}^{\mathrm{BB}} = \mathbf{0}, \tag{B.3}$$

$$\boldsymbol{\tau}^{\mathrm{L}}\,\mathbf{G}^{\mathrm{LB}} + \left[(\varepsilon + \mathrm{i}\eta)\mathbf{1} - \mathbf{H}^{\mathrm{BB}}\right]\mathbf{G}^{\mathrm{BB}} + \boldsymbol{\tau}^{\mathrm{R}}\,\mathbf{G}^{\mathrm{RB}} = \mathbf{1}, \tag{B.4}$$

$$\left(\boldsymbol{\tau}^{\mathrm{R}}\right)^{\dagger}\mathbf{G}^{\mathrm{BB}} + \left[(\varepsilon + \mathrm{i}\eta)\mathbf{1} - \mathbf{H}^{\mathrm{RR}}\right]\mathbf{G}^{\mathrm{RB}} = \mathbf{0}, \tag{B.5}$$

respectively. Here we have introduced the notation

$$\boldsymbol{\tau}^{\mathrm{L}} \equiv -\mathbf{H}^{\mathrm{BL}} = -\left(\mathbf{H}^{\mathrm{LB}}\right)^{\dagger}, \qquad \boldsymbol{\tau}^{\mathrm{R}} \equiv -\mathbf{H}^{\mathrm{BR}} = -\left(\mathbf{H}^{\mathrm{RB}}\right)^{\dagger}, \tag{B.6}$$

to describe the coupling between the interior region $\mathcal{B}$ and the semi-infinite external leads, and exploited the fact that $\mathbf{H}$ is Hermitian. During the discretization process we take these links to be a *nearest neighbour* coupling (see (C.4)) [11]. We also used the fact that the left lead and the right lead are not connected directly, but only through the box i.e.

$$\mathbf{H}^{\mathrm{LR}} = \mathbf{H}^{\mathrm{LR}} = \mathbf{0}. \tag{B.7}$$

Using (B.3) and (B.5) we express the operators $\mathbf{G}^{\mathrm{LB}}$ and $\mathbf{G}^{\mathrm{RB}}$ as

$$\mathbf{G}^{\mathrm{LB}} = -\left[(\varepsilon + \mathrm{i}\eta)\mathbf{1} - \mathbf{H}^{\mathrm{LL}}\right]^{-1}\left(\boldsymbol{\tau}^{\mathrm{L}}\right)^{\dagger}\mathbf{G}^{\mathrm{BB}} = -\mathbf{g}^{\mathrm{L}}\left(\boldsymbol{\tau}^{\mathrm{L}}\right)^{\dagger}\mathbf{G}^{\mathrm{BB}}, \tag{B.8}$$

$$\mathbf{G}^{\mathrm{RB}} = -\left[(\varepsilon + \mathrm{i}\eta)\mathbf{1} - \mathbf{H}^{\mathrm{RR}}\right]^{-1}\left(\boldsymbol{\tau}^{\mathrm{R}}\right)^{\dagger}\mathbf{G}^{\mathrm{BB}} = -\mathbf{g}^{\mathrm{R}}\left(\boldsymbol{\tau}^{\mathrm{R}}\right)^{\dagger}\mathbf{G}^{\mathrm{BB}}, \tag{B.9}$$

where we identified the Green's function $\mathbf{g}^{\mathcal{D}}$ of the *isolated semi-infinite leads* by

$$\mathbf{g}^{\mathcal{D}}(\varepsilon) \equiv \left[(\varepsilon + \mathrm{i}\eta)\mathbf{1} - \mathbf{H}^{\mathcal{D}\mathcal{D}}\right]^{-1}, \qquad \mathcal{D} = \mathrm{L\ or\ R}. \tag{B.10}$$

Substituting both of these into (B.4) we get:

$$\left[(\varepsilon + \mathrm{i}\eta)\mathbf{1} - \mathbf{H}^{\mathrm{BB}} - \boldsymbol{\tau}^{\mathrm{L}}\mathbf{g}^{\mathrm{L}}\left(\boldsymbol{\tau}^{\mathrm{L}}\right)^{\dagger} - \boldsymbol{\tau}^{\mathrm{R}}\mathbf{g}^{\mathrm{R}}\left(\boldsymbol{\tau}\mathrm{R}\right)^{\dagger}\right]\mathbf{G}^{\mathrm{BB}} = \mathbf{1}. \tag{B.11}$$

Accordingly the Green's function in the box is

$$\mathbf{G}^{\mathrm{BB}}(\varepsilon) = \left[\varepsilon\mathbf{1} - \mathbf{H}^{\mathrm{BB}} - \boldsymbol{\Sigma}(\varepsilon)\right]^{-1}. \tag{B.12}$$

It is customary to call the correction term $\boldsymbol{\Sigma} \equiv \boldsymbol{\Sigma}^{\mathrm{L}} + \boldsymbol{\Sigma}^{\mathrm{R}}$ the self-energy [2, 11], where according to (B.11) the definition of $\boldsymbol{\Sigma}^{\mathcal{D}}$ is

$$\boldsymbol{\Sigma}^{\mathcal{D}} \equiv \boldsymbol{\tau}^{\mathcal{D}}\,\mathbf{g}^{\mathcal{D}}\left(\boldsymbol{\tau}^{\mathcal{D}}\right)^{\dagger}. \tag{B.13}$$

This is a very general scenario: if we are only interested in quantities in some 'inner' region ($\mathbf{G}^{\mathrm{BB}}$) and we know the coupling terms to the 'outer' regions ($\boldsymbol{\tau}^{\mathcal{D}}$), then the effect of the latter can be taken into account exactly by self energy terms $\boldsymbol{\Sigma}^{\mathcal{D}}$ [2, 16].

The remaining problem is to calculate $\boldsymbol{\Sigma}^{\mathcal{D}}(\varepsilon)$ for our specific problem. In coordinate representation we have a well known analytical result for the Green's function of an isolated semi-infinite lead when $s = s'$ (see [2]):

$$g_{\varepsilon}^{\mathcal{D}}(s, \varphi; s, \varphi') = -\sum_{m=-\infty}^{\infty}\frac{\sin\left(k_m s\right)}{k_m}\,\phi_m(\varphi)\,\phi_m^{*}(\varphi')\,\mathrm{e}^{\mathrm{i}k_m s}. \tag{B.14}$$

This can be calculated either by using an eigenfunction expansion on $g_{\varepsilon}^{\mathcal{D}}$ and then contour integration techniques or directly from (24) implementing the closed boundary on one side correctly.

Appendix C. Discretization of the problem on a lattice

By introducing a discrete lattice the vanishing of the wavefunction along a strange shaped boundary—like the one in figure 2—is naturally taken into account. Also the $\boldsymbol{\tau}^{\mathcal{D}}$ couplings between region $\mathcal{B}$ and the semi-infinite leads L and R are easy to express, taking the usual nearest neighbour approximation of second derivatives in the Hamiltonian. In continuous-coordinate representation this is a more subtle question [17].

Introducing a two-dimensional lattice with step size Δs and $\Delta\varphi$ in the s and φ directions respectively we represent the wavefunctions on the $|i\rangle$ basis of lattice points as

$$|\Psi\rangle = \sum_i \Psi[i]\ |i\rangle \qquad \text{with} \quad \Psi[i] \equiv \sqrt{\Delta s \Delta\varphi}\ \Psi(s_i, \varphi_i), \tag{C.1}$$

where (s_i, φ_i) are the coordinates of lattice point i. The Hamiltonian of (5) taking the nearest neighbours in the second derivatives are given by a matrix with elements

$$H[i, j] = \begin{cases} 2\left(1/\Delta s^2 + 1/\Delta\varphi^2\right), & \text{if } i = j, \\ -1/\Delta s^2 \text{ or } -1/\Delta\varphi^2, & \text{if } i \text{ and } j \text{ are nearest neighbours} \\ 0, & \text{otherwise.} \end{cases} \tag{C.2}$$

The Green's function is represented as the matrix

$$\mathbf{G}(\varepsilon) = \sum_{i,j} G_{\varepsilon}[i, j]\,|i\rangle\langle j\,|, \qquad \text{with} \quad G_{\varepsilon}[i, j] = G_{\varepsilon}\left(s_i, \varphi_i; s_j, \varphi_j\right)\Delta s \Delta\varphi. \tag{C.3}$$

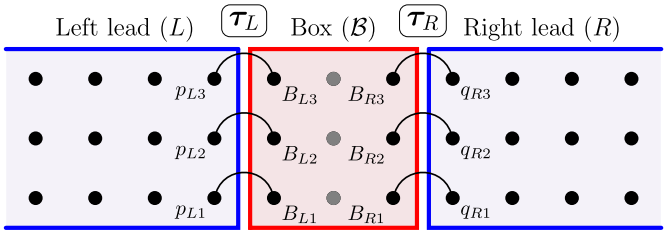

Figure C1. Representation of the partitioning, introducing a notation on the adjacent points of different parts showing schematically the coupling terms connecting the finite region $\mathcal{B}$ to the semi-infinite leads L and R.

From (C.2) with the notations of figure C1 the couplings (B.6) between $\mathcal{B}$ and the leads are:

$$\boldsymbol{\tau}^{\mathrm{L}} = \frac{1}{\Delta s^2}\sum_{i\in \mathrm{L}} \left|\mathrm{B}_{\mathrm{L}i}\right\rangle \left\langle p_{\mathrm{L}i}\right|, \qquad \boldsymbol{\tau}^{\mathrm{R}} = \frac{1}{\Delta s^2}\sum_{i\in \mathrm{R}} \left|\mathrm{B}_{\mathrm{R}i}\right\rangle \left\langle q_{\mathrm{R}i}\right|. \tag{C.4}$$

From (C.4) we calculate the $\boldsymbol{\Sigma}$ correction (exactly) on the lattice. Focusing on $\boldsymbol{\Sigma}^{\mathrm{R}}$ we see that according to the definition (B.10) the transformation with $\boldsymbol{\tau}^{\mathrm{R}}$ 'picks out' those elements of $\mathbf{g}^{\mathrm{R}}$ which correspond to the $(p_{\mathrm{R}i}, p_{\mathrm{R}j})$ points, i.e. the end points of the semi-infinite domain (see figure C1). Nonzero elements of $\boldsymbol{\Sigma}^{\mathrm{R}}$ are

$$\boldsymbol{\Sigma}^{\mathrm{R}}_{\varepsilon}\left[\mathrm{B}_{\mathrm{R}i}, \mathrm{B}_{\mathrm{R}j}\right] = \frac{1}{\Delta s^4}\, g^{\mathrm{R}}_{\varepsilon}\left[p_{\mathrm{R}i}, p_{\mathrm{R}j}\right] = -\frac{1}{\Delta s^2}\sum_{m=-\infty}^{\infty} \phi_m\left[p_{\mathrm{R}i}\right] \mathrm{e}^{\mathrm{i}k_m \Delta s}\, \phi^{\star}_m\left[p_{\mathrm{R}j}\right]. \tag{C.5}$$

We note that for a discrete lattice the dispersion relation is modified, the k_m in (B.10) has to be replaced by $k_m = \sin\,(k_m \Delta s)/\Delta s$.

In this way the finite size matrix to be inverted for $\mathbf{G}^{\mathrm{BB}}$ in (26) is fully defined.

References

[1] Shore B W, Dömötör P, Süssmann G, Sadurní E and Schleich W P 2015 Scattering of a particle with internal structure from a single slit *New J. Phys.* **17** 013046
[2] Datta S 1995 *Electronic Transport in Mesoscopic Systems* (*Cambridge Studies in Semiconductor Physics and Microelectronic Engineering*) (Cambridge: Cambridge University Press)
[3] Souma S and Suzuki A 2002 Local density of states and scattering matrix in quasi-one-dimensional systems *Phys. Rev.* B **65** 115307
[4] Economou E N 2006 Green's functions in quantum physics *Springer Series in Solid-State Sciences* (Berlin: Springer)
[5] Feshbach H 1958 Unified theory of nuclear reactions *Ann. Phys., NY* **5** 357–90
[6] Feshbach H 1962 A unified theory of nuclear reactions: II. *Ann. Phys., NY* **19** 287–313
[7] Callaway J 1967 *t* matrix and phase shifts in solid-state scattering theory *Phys. Rev.* **154** 515–21
[8] Domcke W 1991 Theory of resonance and threshold effects in electron-molecule collisions: the projection-operator approach *Phys. Rep.* **208** 97–188
[9] Dennery P and Krzywicki A 1967 *Mathematics for Physicists* (New York: Dover)
[10] Lippmann B A and Schwinger J 1950 Variational principles for scattering processes: I. *Phys. Rev.* **79** 469–80
[11] Di Ventra M 2008 *Electrical Transport in Nanoscale Systems* (Cambridge: Cambridge University Press)
[12] Fisher D S and Lee P A 1981 Relation between conductivity and transmission matrix *Phys. Rev.* B **23** 6851–4
[13] Ferry D K, Goodnick S M and Bird J P 2009 *Transport in Nanostructures* 2 edn (Cambridge: Cambridge University Press)
[14] Jackson J D 1999 *Classical Electrodynamics* (New York: Wiley)
[15] Kaplan W 1984 *Advanced Calculus* (Reading, MA: Addison-Wesley)
[16] Datta S 2000 Nanoscale device modeling: the Green's function method *Superlattices Microstruct.* **28** 253–78
[17] Caroli C, Combescot R, Lederer D, Nozieres P and Saint-James D 1971 A direct calculation of the tunnelling current: II. Free electron description *J. Phys. C: Solid State Phys.* **4** 2598